3rd Symposium on Heat Resistant Steels and Alloys for High Efficiency USC Power Plants 2009
National Institute for Materials Science, Tsukuba , Japan, June 2-4, 2009

Experience with 9Cr3W3CoVNbBN Base Material and Crosswelds at 650°C for Implementation in USC Power Plants

Peter Mayr[1], Ivan Holzer[1], Francisca Mendez-Martin[1], Alina Agüero[2], Vanessa González[2], Susanne Baumgartner[3] and Horst Cerjak[1]

[1] Institute for Materials Science and Welding, Graz University of Technology, Kopernikusgasse 24, 8010 Graz, Austria, peter.mayr@tugraz.at

[2] Instituto Nacional de Técnica Aeroespacial, Ctra. de Ajalvir Km 4, 28850 Torrejón de Ardoz, Spain

[3] Böhler Schweißtechnik Austria GmbH, Böhler-Welding-Str. 1, 8605 Kapfenberg, Austria

ABSTRACT

This manuscript gives an overview on recent developments of a martensitic steel grade based on 9Cr3W3CoVNb with controlled additions of boron and nitrogen. Alloy design by thermodynamic equilibrium calculations and calculation of boron-nitrogen solubility is discussed.

Two melts of a 9Cr3W3CoVNb steel were produced. The oxidation resistance was examined at 650°C in steam atmosphere. The alloy exhibited high resistance to steam oxidation at 650°C for at least 5.000 hours of exposure.

Microstructural evolution during welding within the heat-affected zone was investigated by physical weld simulation, thermo-dilatometry and in situ X-ray diffraction using high energy synchrotron radiation. The heat-affected zone microstructure is characterized by optical microscopy. Two multilayer welds, one with a nickel based filler and one with a newly developed flux cored filler of matching chemical composition, were fabricated. All weldability experiments showed that within the heat-affected zone the initial base material microstructure is retained to a large extent. The formation of a uniform fine-grained heat-affected zone region is suppressed.

Uniaxial creep tests of base material, weld metal and crossweld specimens were started at different levels of stress at 650°C. Up to the established maximum testing time of 20.000 hours, the base material shows significant improvement compared to standard 9 wt. % Cr grades P91 and P92. Crossweld specimens show an improved strength level, higher than that of grade P92 base material.

Preliminary results of an extensive testing program on a 9Cr3W3CoVNbBN steel show significant improvement compared to the state-of-the-art 9 wt. % Cr martensitic steel grades.

1. Introduction

In Japan and Europe, research and development works in the field of advanced martensitic creep resistant steels has a long history [1-3]. The fields of application for such materials are especially large diameter and thick section boiler components, such as main steam pipes and headers of ultra-supercritically (USC) operated plants. The target of steel development is defined by a creep rupture strength of 100 MPa after 100.000 hours at 650°C. Beside high creep rupture strength, also high steam oxidation resistance at service temperature, acceptable thermal cycling capabilities, i.e. fatigue strength, and also good formability and weldability are mandatory for new martensitic creep resistant steel grades.
Within the last years, the alloy design philosophy for martensitic steels strongly targets the long-term stability of microstructure [4]. Migration of lath and block boundaries, causing the coarsening of martensite laths and blocks by annihilation of excess dislocations, closely correlates with the onset of accelerated creep. A fine dispersion of $M_{23}C_6$ and MX particles, which exert a pinning force on migrating boundaries and dislocations, has been identified as main contributor in suppressing recovery of the martensitic microstructure.
The work presented in this manuscript is following an extensive research program started at the National Institute for Materials Science (NIMS), Japan [4]. In detail, the NIMS alloy design concept follows stabilization of $M_{23}C_6$ carbides and grain boundaries by the addition of boron in combination with finely dispersed MX particles as a possible solution to stabilize the martensitic substructure. As basis for the systematically study of the influence of boron and nitrogen on long term creep behavior, a Fe-0.08C-9Cr-3W-3Co-0.2V-0.05Nb (wt. %) steel with different concentrations of boron and nitrogen was investigated [5,6].

The influence of boron on 9Cr3W3CoVNb steel was studied in the range of 0 to 140 ppm (parts per million) while nitrogen level was kept constant at a minimum between 10 to 30 ppm [5]. The influence of boron on creep properties was studied by uniaxial-creep testing at 650°C at different stress levels. At stress levels higher than 100 MPa, no big difference in creep strength between 0B, 0.0048B and 0.0092B steel was found. Only 0.0139B steel showed improved creep strength. While at lower stress levels, creep strength of the lower boron steels decreased significantly, 0.0139B steel showed a stable creep behavior. It was concluded that controlled addition of boron can delay the decrease of long-term creep strength in 9Cr3W3CoVNb steel. As a result of the boron series creep tests, a boron content of 140 ppm was identified as optimum for improved creep behavior.
The combined effect of boron plus additional MX precipitation was studied by 9Cr3W3CoVNb test melts with a fixed boron content of 140 ppm and varying nitrogen levels of 15, 79 and 650 ppm [6]. Increasing the nitrogen level to 79 ppm resulted in further improvement of the creep strength of the base 9Cr3W3CoVNb-0.0140B steel. However, further increase of nitrogen to 650 ppm showed no beneficial effects and in turn reduced creep strength of the alloy.
The main idea behind the NIMS alloying concept is to combine boron-strengthening with nitride-strengthening. However, excess addition of nitrogen in combination with boron causes the formation of boron nitrides (BN) during forming and heat treatments at elevated temperatures. Precipitation of boron nitrides offsets the beneficial effect of boron and nitrogen addition. Sakuraya et. al [7] showed in their work on BN formation in high Cr heat resistant steels that, a particular relationship between boron and nitrogen has to be kept to avoid

formation of coarse BN particles. From experimental observations the authors derived a formulation for the solubility product of BN.
Also weldability of 9Cr3W3CoVNb steel was investigated by several researchers [8,9]. Creep rupture data at 650°C for crosswelds of 9Cr3W3CoVNb steel with addition of 130 ppm boron and low nitrogen content of 15 ppm, standard P92 and P91-type steel was compared to creep rupture data of their base metals. There was basically no degradation of creep rupture strength in the 9Cr3W3CoVNbB-low N steel welded joints, while degradation of creep strength of P92 welded joints became more significant with increasing test duration. This behavior was attributed to the suppression of a grain refined region in the heat-affected zone (HAZ) of the 9Cr3W3CoVNbB-low N steel. The responsible mechanism discussed are austenite memory effect and martensitic reverse transformation [9].

Within the present work, the NIMS alloy design regarding the optimum boron-nitrogen relationship was slightly modified based on thermodynamic studies. On the following pages the alloy design for a boron and nitrogen strengthened 9Cr3W3CoVNb steel is described in detail and first results of creep tests, oxidation test and welding trials are presented.

2. Experimental

Alloy Design. Thermodynamic equilibrium calculations were performed using the software Matcalc [10-13] utilizing the thermodynamic database Fe-data6 [14]. The description of BN in the database was slightly modified, based on the work of Fountain et al. [15].

Materials. A 20 kg heat (Heat 1) of 9Cr3W3CoVNb steel with controlled additions of 120 ppm boron and 130 ppm nitrogen was produced by vacuum induction melting. The addition of boron and nitrogen was set to avoid the formation of large boron nitrides but still allow the precipitation of strengthening MX particles. For homogenization of Heat 1, the ingot (110 mm square) was forged to final dimensions of 50 mm square. A second heat (Heat 2) of a 9Cr3W3CoVNb steel with slightly reduced boron (110 ppm) and nitrogen (110 ppm) content was produced and rolled to 20 mm thick plates. The exact chemical composition in weight % (wt. %) of Heat 1 and Heat 2 is given in Table 1. The final quality heat treatment for both heats consisted of normalizing at 1150 °C for 1 hour followed by tempering at 770 °C for 4 hours.

Table 1: Chemical composition of 9Cr3W3CoVNbBN test melts in wt. % (balanced Fe).

Analysis	C	Si	Mn	Cr	W	Co	V	Nb	B	N
Heat 1	0.074	0.29	0.44	9.26	2.84	2.95	0.21	0.056	0.012	0.013
Heat 2	0.090	0.30	0.51	9.26	2.92	2.88	0.20	0.050	0.011	0.010

Within this manuscript, data on Heat 2 is exclusively limited to welding trials using a newly developed chemically matching martensitic weld metal. All data reported on microstructural characterization, oxidation and creep testing is related to Heat 1.

Welding Trials. To investigate the weldability of the newly developed steel and the creep behavior of crossweld specimens, two plates of Heat 1 were welded by gas tungsten arc welding (GTAW) process using a nickel based filler metal (Nibas 70/2-IG). A nickel based

filler metal was chosen, as at that time, no martensitic filler material with sufficient creep strength was available and fracture would always have occurred in the weld metal. Details regarding the welding procedure can be found in [16].
A second weld was produced of Heat 2 material using a flux-cored wire with chemically matching composition, which was developed within the current project. Postweld heat treatment for both welds was carried out at 740°C for 4 hours.

Steam Oxidation Laboratory Testing. The schematics of the closed loop laboratory rig employed at INTA are shown elsewhere [17]. Prior to testing, laboratory air is displaced from the chamber by means of N_2 which is kept flowing while heating up to the test temperature (approximately at 600ºC/h). Once the test temperature is reached, the N_2 flow is closed and pure steam is introduced at a linear velocity of 8 cm/s. To carry out weight measurements or to remove samples, the furnace is cooled to about 300ºC under N_2 atmosphere and the specimens are subsequently removed. The reheat cycle is also carried out under N_2 atmosphere.

Characterization. Base material microstructure was characterized by light optical microscopy, scanning electron microscopy (SEM) and analytical transmission electron microscopy (TEM). Details are reported in [18]. The oxidized specimens were characterized by optical and field emission scanning electron microscopy (FESEM) employing a JEOL JSM 840 system equipped with an energy dispersive X-ray spectrometer (EDS) KEVEX MICROANALYST 8000 with a RÖNTEC signal processor.

3. Modified Alloy Design Concept

To take advantage of boron and nitrogen addition the formation of large boron nitrides (BN) has to be avoided. Therefore, in the present work the allowable boron and nitrogen limits for high chromium martensitic steels were determined by thermodynamic equilibrium calculations. Within this study, the BN solubility product for a 9Cr3W3CoVNbBN steel, based on the chemical composition of Heat 1, was calculated for various B/N ratios and different temperatures (representative for normalizing), considering also possible formation of boride (M_2B).
The result is shown in Figure 1. The solubility products (solid lines) are shown for different temperatures ranging from 900°C to 1250°C. The dashed grey lines show the solubility product for the M_2B phase. Furthermore, the BN solubility line reported by Fountain et al. [15] at 1150°C and Sakuraya et al. [19] are included in the figure.
The grey areas in Figure 1 indicate the critical B/N ratios where BN formation is predicted. No formation of BN is expected below the respective BN solubility line. Figure 1 clearly shows that the experimental findings reported by Sakuraya et al. [19] are well described by the thermodynamic equilibrium considerations in the temperature range between 900°C and 1250°C. For the B/N ratios reported by Sakuraya et al. [7] no BN formation is predicted for temperatures higher than 1250°C, consistent with the experimental findings.
Due to the temperature dependence of the BN solubility product it can be assumed that coarse BN (>1µm) exist for high boron and nitrogen contents and low normalizing temperatures. This leads to the conclusion that in Heat 1 only small and in Heat 2 no BN should form.

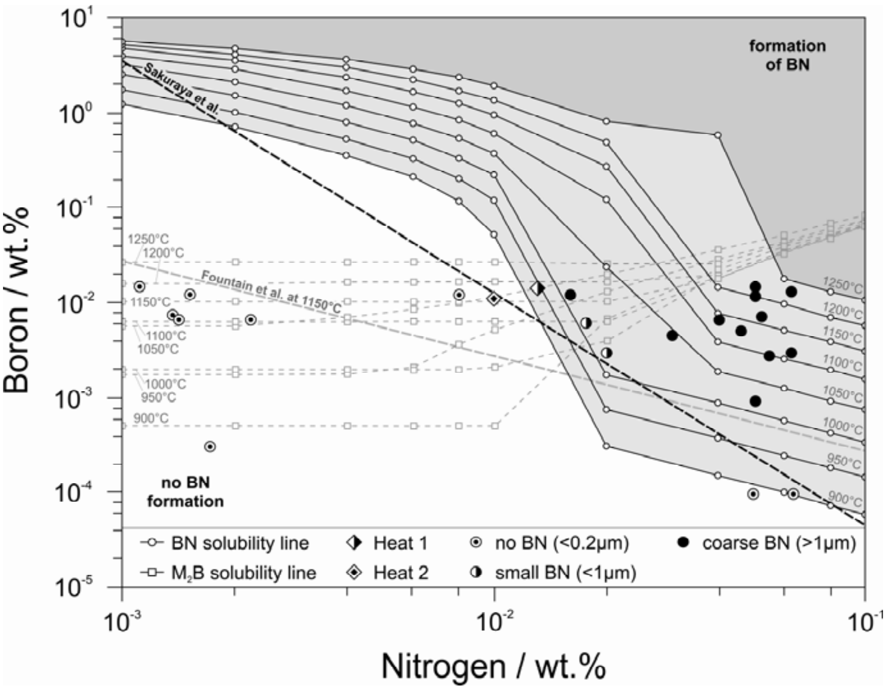

Figure 1: BN solubility product for a 9Cr3W3CoVNbBN steel as a function of temperature in the range between 900°C and 1250°C. The grey areas indicate the range of BN formation at high temperatures. The calculation is compared to the solubility products reported by Sakuraya et al. [19] and Fountain et al. [15].

4. Microstructure of 9Cr3W3CoVNbBN steel

Optical micrographs of 9Cr3W3CoVNbBN base material (Heat 1) show a tempered martensitic microstructure (see Figure 2). The average prior austenite grain size is 250 µm in diameter and precipitates are finely distributed mainly along prior austenite grain and martensite lath boundaries.

Via electron microscopy, MX (V,Nb)(N,C) carbonitrides and $M_{23}C_6$ $(Cr,Fe,Mo,W)_{23}C_6$ carbides have been identified at grain and lath boundaries and/or in the matrix of the base material. MX (V,Nb)(N,C) particles have a representative diameter smaller than 100 nm and Cr-rich carbides have a diameter between 150 and 250 nm. By SEM and EDS only very few and small (<1µm) BN particles for Heat 1 and no BN particles for Heat 2 have been detected. A detailed description of the method of detecting BN particles is given in [19]. These experimental findings support the results of the thermodynamic equilibrium calculations in the alloy design stage.

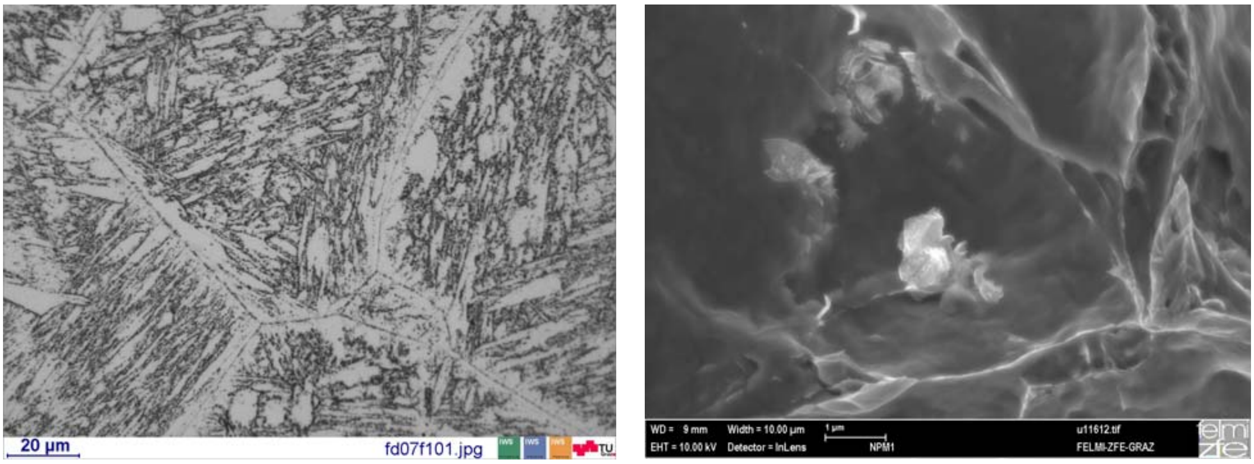

Figure 2: Optical micrograph of normalized and tempered 9Cr3W3CoVNbBN base material (left) and small BN particle (right) identified by EDS - both images for Heat 1.

After creep exposure for 8.971 hours at 650 °C and 130 MPa light-optical and electron microscopical investigations have been performed. The prior austenite grain and martensite lath structure, after almost 10.000 h of creep, show no significant changes. The precipitate size and number density of carbonitrides and carbides remain almost the same as in the base material. The electron microscopy investigation reveals the precipitation of two new phases: laves phase (intermetallic phase A_2B, $(Fe,Cr)_2(W,Mo)$ with approximately 38 atom % of tungsten and more than 45 atom % of iron, distributed mainly at the grain boundaries and modified Z-phase (complex nitride [(Cr,V,Nb)N]) with a very low phase fraction. Details on the microstructural evolution of 9Cr3W3CoVNbBN steel during creep exposure can be found in [20].

5. Oxidation behavior

Specimens of 9Cr3W3CoVNbBN (Heat 1) were exposed to pure, flowing steam at 650ºC for 4.908 h. Figure 3 shows the mass variation of the new steel as function of time as well as that of 9 wt.% ferritic steels P91 and P92 for comparison purposes. 9Cr3W3CoVNbBN exhibits a mass gain considerably lower than that of the other two 9 wt. % Cr steels. This behavior is surprising, as work done by several research groups have indicated the steam oxidation resistance of steels correlates strongly with the Cr contents, and results so far have indicated that 9 wt. % Cr steels oxidized very fast when exposed to steam at T > 600ºC [21-24]. For instance, Quadakkers and collaborators have concluded that a Cr wt.% of 11 or more is required to form a protective scale [21].

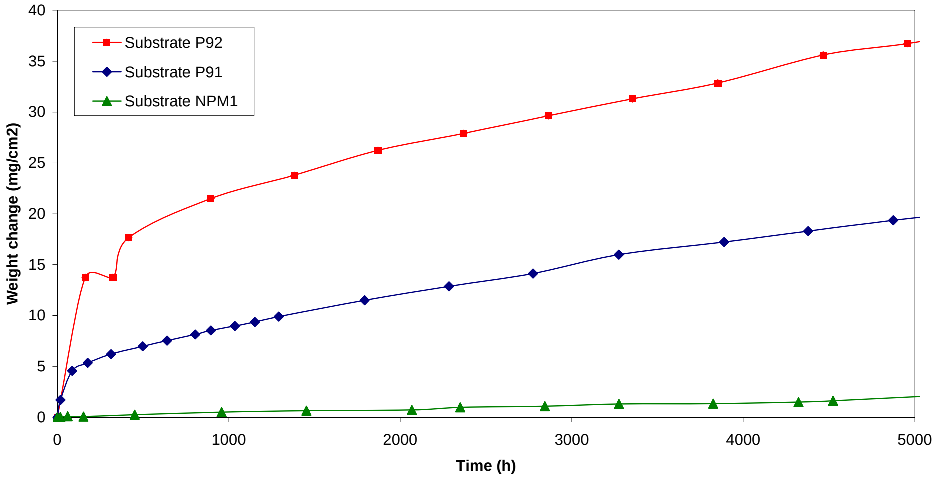

Figure 3: Mass variation of substrates exposed to flowing steam (1 bar) at 650º C

Figure 4 shows an image of a specimen exposed 4.908 h. Nodular features can be observed, especially at the samples edges but most of the surface appears smooth. On the cross section of the exposed surface a very thin (< 100 nm) Cr and O rich layer, most likely Cr_2O_3 can be observed with difficulty.

This type of oxide is typical of steels containing 11 wt. % of Cr. Quadakkers found that Co tends to increase the oxidation resistance of 9-12 Cr wt. % ferritic steels [21], but not to the extent observed for 9Cr3W3CoVNbBN. On the other hand, other groups have observed that the higher the W content the lower the oxidation resistance of this type of steels [22,25,26]. It is therefore not clear yet why this 9 wt. % steel exhibits such high steam oxidation resistance and further studies are required.

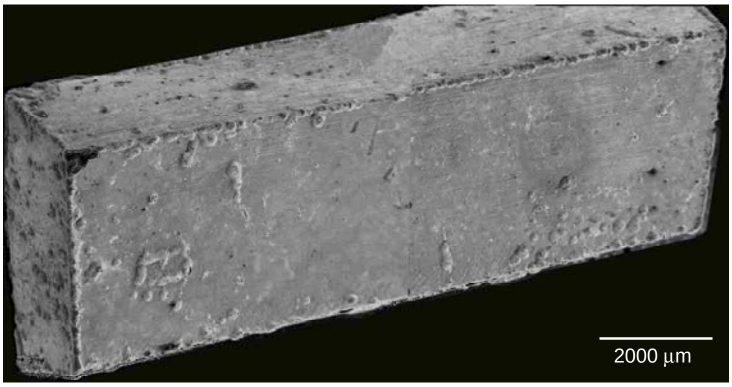

Figure 4: SEM image of a 9Cr3W3CoVNbBN specimen exposed to steam at 650ºC for 4.908 h

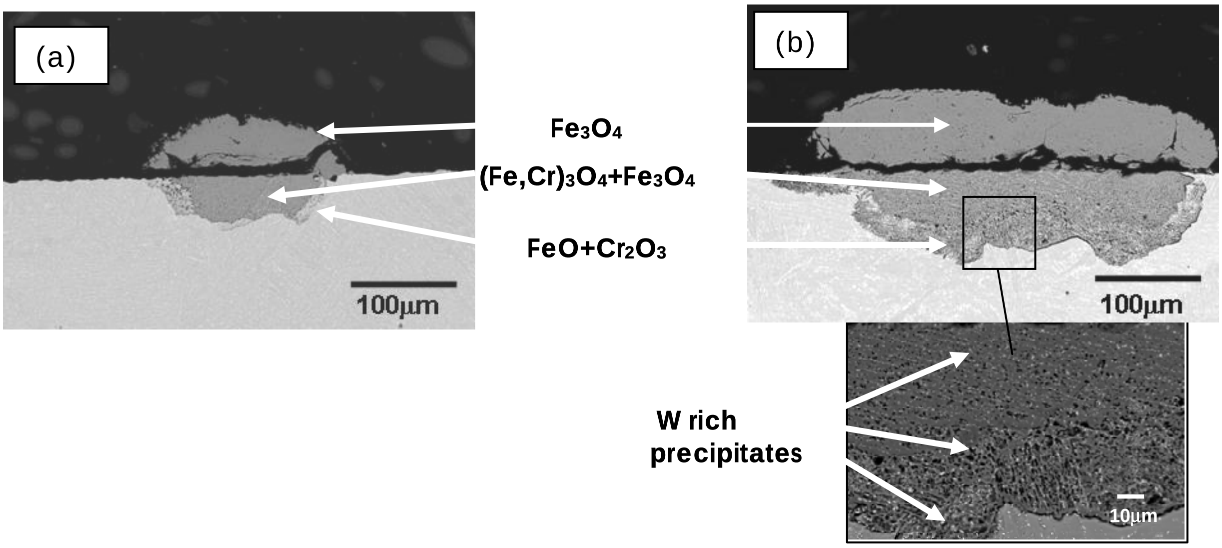

Figure 5: FESEM image of the cross section of 9Cr3W3CoVNbBN exposed to steam at 650ºC at a nodule site: (a) for 1.260 h, (b) for 4.908 h

The cross section of representative nodules formed after 1.260 and 4.908 h are shown in Figure 5a and b respectively. The microstructure corresponds to a dual oxide layer similar to that observed on ferritic steels containing 9 wt.% in Cr, with a top outwards growth Fe_3O_4 layer and an inner growing mixed oxide layer containing (Fe, Cr)$_3$O$_4$, FeO and Cr_2O_3 [27] which also contains W, Co and V. Interestingly, W rich nanoscale precipitates which are also present in the substrate can be observed in this inner oxide layer. The nodules in the 1.260 h specimen exhibit lower thickness and width than those observed in the specimen exposed for 4.908 h, indicating that these oxides are growing fast and therefore are not protective, and moreover, the number of nodules on the 4.908 h is higher than that observed on the 1.260 h specimen.

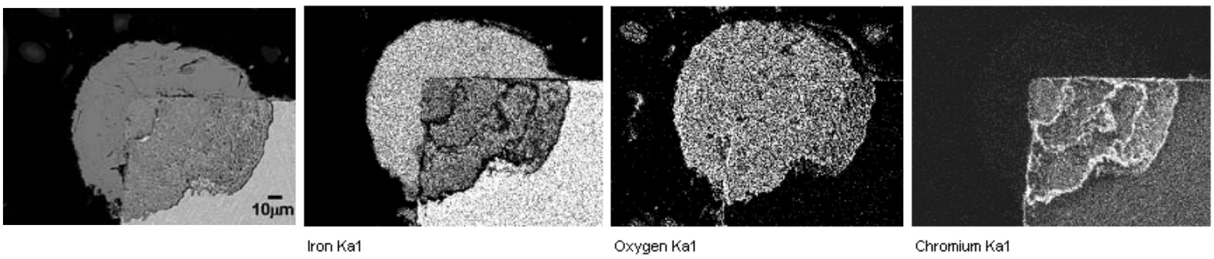

Figure 6: Cross section of the edge of a 9Cr3W3CoVNbBN specimen exposed to steam oxidation at 650º C for 4.908 h

At the specimen's edge (Figure 6) the corresponding EDS composition map reveals Cr rich layers within the inner oxide and the original specimen surfaces can be clearly observed. The average Cr content (19 wt. %) in this inner oxide zone is significantly higher than that of the substrate, but because it is not uniformly distributed as shown, it is not protective. According to Quaddakers and coworkers, this pattern results from the repetition of cycles in which Cr rich spinels form due to rapid Cr diffusion from the bulk alloy until the spinel cannot be sustained due to continuous Cr depletion, resulting in the formation of Fe rich oxides [21]. Formation of oxidation nodules has been observed on oxidation resistant 12 wt. % steels and has been attributed to compositional inhomogeneities [21,28]. For this 9Cr steel the presence of nodules can be rather attributed to local cracks, imperfections and/or rupture of the protective scale on a Cr depleted substrate. The fact that the samples edges are fully covered with nodules support this hypothesis as due the higher residual stresses, corners and edges are more prone to develop cracks.

6. Weldability

The transformation behavior and weldability of 9Cr3W3CoVNbBN steel was investigated by thermo-dilatometry, in-situ X-ray diffraction using synchrotron radiation [29] and physical heat-affected zone (HAZ) simulation using a Gleeble thermo-mechanical simulator. Additionally, two welded joints were produced, one with a Ni-based filler (Heat 1) and one with compositional matching flux-cored wire (Heat 2).

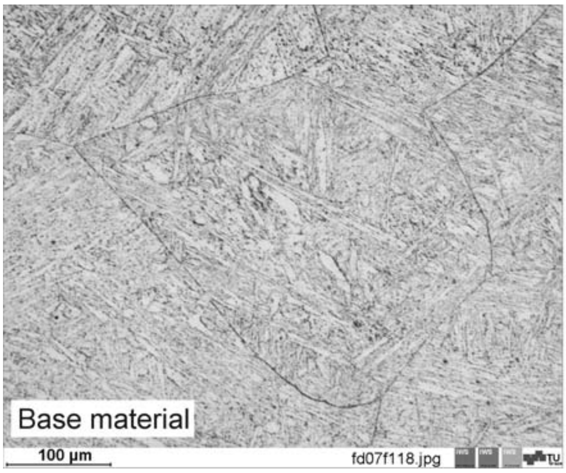

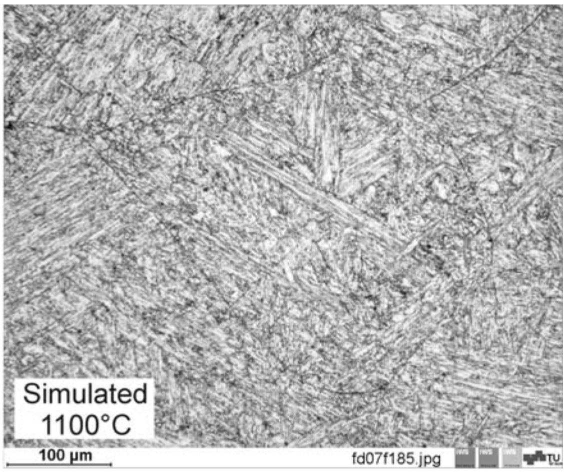

Figure 7: Comparison of the NPM1 microstructure at the same location before and after HAZ simulation applying a peak temperature of 1100°C revealing no grain refinement during the weld thermal cycle.

Applying a heating rate of 100°C/s resulted in an A_{c1} temperature of 909°C and a A_{c3} of 1028°C. Therefore, heating a sample to a peak temperature of 1100°C results in complete austenitisation and martensitic transformation on subsequent cooling (cooling rate 100°C/s). The onset of martensite formation (M_s) was measured at 488°C. Although, the steel undergoes two phase transformations during such thermal cycle, the initial grain structure is almost retained completely. Identical prior austenite grain boundaries and martensitic lath structure can be observed before (Figure 7 left) and after thermal HAZ simulation (Figure 7 right). 9Cr3W3CoVNbBN steel does not form a uniform fine-grained HAZ region.

Within this work, a matching flux cored wire of matching chemical composition for a 9Cr3W3CoVNbBN steel was developed. Flux cored wires in general combine the beneficial effects of covered stick electrodes like slag metallurgy, protection of the weld pool by a slag and improved out of position weldability with the advantage of solid wires to be used in automatic and robotic welding applications. To assure good welding behavior and out of position weldability a rutile (TiO_2) slag system has been designed. This slag concept has already been applied successfully to other creep resistant flux cored wires. Special focus for the 9Cr3W3CoVNbBN filler has been put on the adjustment of the boron and nitrogen content. The welding procedure resulted in a sound and defect free weld (Figure 8).

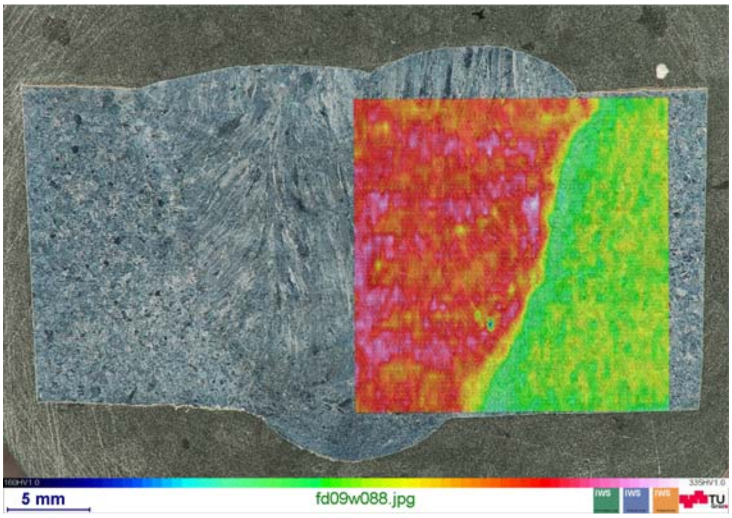

Figure 8: 9Cr3W3CoVNbBN steel (Heat 2) welded with filler metal of matching composition and corresponding hardness mapping (blue corresponds to 160HV1 and white to 335 HV1) after PWHT of 740°C for 4 hours.

7. Creep Strength

Uniaxial creep tests of 9Cr3W3CoVNbBN base material, weld metal and crossweld specimens have been carried out at 650°C. At present, the longest running creep test of base material has reached 21.000 hours at 100 MPa, as shown in Figure 9. The base material tested at a higher stress level of 130 MPa fractured after 8.971 h. This results in an improvement of rupture stress at approximately 9.000 hours of +60 MPa and +40 MPa compared to grades P91 and P92 respectively.

Pure weld metal specimens of type 9Cr3W3CoVNbBN were tested at 650°C and 150 MPa solely for creep strength screening purpose. The pure weld metal specimens exhibit similar short term creep rupture strength as the base material.

Results of creep tests of crossweld specimens are only available for the weld produced with Ni-base filler metal. Tests have reached a maximum duration of more than 11.000 hours. Three crossweld samples have fractured so far. Crossweld creep rupture data shows a significant improvement compared to the mean creep strength of base material P91 and P92. Specimens tested at stresses lower than 100 MPa are still running.

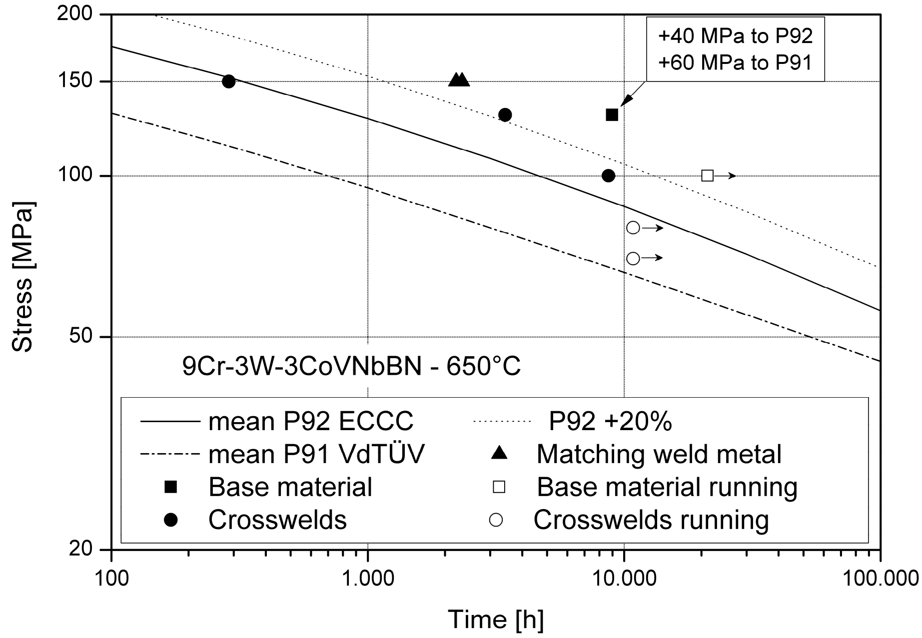

Figure 9: Creep testing data of 9Cr3W3CoVNbBN base material, weld metal and crosswelds at 650°C compared to well-established grades P91 and P92.

8. Summary and Conclusions

Alloy design for a 9 wt. % Cr steel has been successfully improved by thermodynamic calculation of phase fraction diagrams and calculation of the boron-nitrogen solubility product. The boron and nitrogen content of a 9Cr3W3CoVNbBN steel was adjusted to have either only very small boron nitrides (Heat 1) or no precipitation of BN (Heat 2).
9Cr3W3CoVNbBN exhibits an unexpected high steam oxidation resistance at 650°C despite its low Cr content. It develops a thin Cr rich protective oxide scale despite its relatively low Cr content. However, oxidation nodules form, very likely due to protective oxide imperfections, growing in thickness, width and number as a function of steam exposure time.
Two welded joints have been successfully produced, one with a Ni-base filler wire and one with a newly developed chemically matching flux-cored filler wire.
Creep tests performed at 650°C of base material, martensitic weld metal and crosswelds show improved creep strength. The increased creep rupture strength of the welded joint can be attributed to the suppressed formation of a fully refined heat-affected zone microstructure.

As a whole, the boron and nitrogen alloyed martensitic 9Cr3W3CoVNbBN steel and its welded joints show very promising creep properties at 650°C and also unexpected high oxidation resistance in steam. The underlying mechanism are currently studied.

9. Acknowledgements

The authors would like to acknowledge the support by the European Cooperation in Science and Technology (COST) through Action 536 "Alloy development for Critical Components of Environmental friendly Power planT (ACCEPT)" and the Austrian Research Promotion Agency (FFG).

10. References

[1] Kern T U, Wieghardt K and Kirchner H, in 4th int conf Advances in Materials Technology for Fossil Power Plants, Hilton Head Island, ASM International, 2005.
[2] Masuyama F, in 4th int conf Advances in Materials Technology for Fossil Power Plants, Hilton Head Island, ASM International, 2005.
[3] Cerjak, H.-H.; Dimmler, G.; Holzer, I.; Kozeschnik, E.; Mayr, P.; Pein, C.; Sonderegger, B.: Materials science forum 539-543 (2007) , S. 2954 - 2959
[4] Abe F, in 4th int conf Advances in Materials Technology for Fossil Power Plants, Hilton Head Island, SC, EPRI, 2004.
[5] Abe F, Horiuchi T and Sawada K, Materials Science Forum, 2003, 426-432, 1393-1398.
[6] Semba H and Abe F, “in 4th int conf Advances in Materials Technology for Fossil Power Plants, Hilton Head Island, SC, EPRI, 2004.
[7]Sakuraya K., Okada H., Abe F., ISIJ Int., vol. 46 (2006), 1712.
[8] Kondo M, Tabuchi M, Tsukamoto S, Yin F and Abe F, in 4th int conf Advances in Materials Technology for Fossil Power Plants, Hilton Head Island, SC, EPRI, 2004.
[9] Kondo M, Tabuchi M, Tsukamoto S, Yin F and Abe F, STWJ, 2006 11(2) 216-223
[10]Kozeschnik E., Buchmayr B., Mathematical Modelling of Weld Phenomena 5, Institute of Materials, London, 2001, 349.
[11]Svoboda J., Fischer F. D., Fratzl P., Kozeschnik E., Mater. Sci. Eng. A, vol 385 (2004) 166.
[12]Kozeschnik E., Svoboda J., Fratzl P., Fischer F. D., Mater. Sci. Eng. A, vol 385 (2004) 157.
[13]Kozeschnik E., Svoboda J., Fischer F. D., CALPHAD, vol 28 (2005) 379.
[14]Saunders M., Fe-data6.tdb.
[15] R.W. Fountain, Chipman J., Transactions of the Metallurgical Society of AIME, vol. 224 (1962) 599.
[16] Mayr P, Cerjak H, Jochum C and Pasternak J: in 8th International Conference on Creep and Fatigue at Elevated Temperatures 2007, San Antonio, 2007
[17]Agüero A., Muelas R., Scarlin B., and Knödler R., Materials for Advanced Power Engineering 2002, Part III (2002), p. 1143
[18]Mayr P., PhD-Thesis, Graz University of Technology, 2007
[19]Sakuraya K., Okada H., Abe F., in: Advances in Materials Technology for Fossil Power Plants: Proceedings of the Fourth International Conference, (2004) 1270.
[20] Mayr, P.; Mendez Martin, F.; Albu, M.; Cerjak, H.-H.: in: Creep and Fracture in High Temperature Components - Design & Life Assessment Issues (2009), S. 1029 - 1037
[21]Quadakkers W.J. and Ennis P.J., Materials for Advanced Power Engineering 1998, Part I (1998) p. 123
[22]Nava-Paz J.C. and Knödler R., Materials for Advanced Power Engineering 1998, Part I (1998) p. 451
[23]Fukuda Y., Tamura K. and Sato T., Materials for Advanced Power Engineering 1998, Part I (1998) p. 461
[24]Ennis P.J. and Quadakkers W.J., Materials for Advanced Power Engineering 2002, Part II (2002) p. 1131
[25]Knödler R. and Scarlin B., Materials for Advanced Power Engineering 2002, Part III (2002) p. 1601
[26]Agüero A. and Muelas R., Materials Science Forum, 461-464 (2004) p. 957
[27]Zurek J., Nieto-Hierro L., Piron-Abellan J., Niewolak L., Singheiser L. and Quadakkers W.J., Materials Sceince Forum, 461-464 (2004) p. 791
[28]Lepingle V., Louis G., Petelot D., Lefevre B. and Vandenberghe B., Materials Science Forum, 461-464 (2004) p. 1039
[29] Mayr, P.; Palmer, T. A.; Elmer, J. W.; Specht, E. D.: International journal of materials research 99 (2008) 4, p. 381 - 387